Proceedings of ISFOG 2025
5TH INTERNATIONAL SYMPOSIUM ON
FRONTIERS IN OFFSHORE GEOTECHNICS
Nantes, France | June 9-13 2025

ISBN 978-2-85782-758-0

Numerical modelling of free fall penetration of a spherical penetrometer in sand

Ankur Singh*
Indian Institute of Technology Bombay /Department of Civil Engineering/Mumbai, India
Santiram Chatterjee
Indian Institute of Technology Bombay /Department of Civil Engineering/Mumbai, India
**214040019@iitb.ac.in*

ABSTRACT:
In the recent past, Free Fall Penetrometers (FFPs) have emerged as useful offshore site exploration tools for characterizing shallow depth sediments. FFPs are simple to design and easy to deploy. Studies have reported the use of different shapes of FFPs for characterizing both sandy and clayey soils. While the use of conical FFP with a shaft is more common in the existing literature, researchers have also reported the use of shaftless spherical FFPs. FFPs deployed in the field are generally fitted with inertial measurement units including accelerometers and gyroscopes. The measured deceleration time history can be related to the mechanical properties and state of the soil. In this paper, Coupled Eulerian Lagrangian formulation of the commercial package Abaqus has been used to simulate the penetration of a spherical FFP in dry sand. The impact of the free-falling sphere is simulated by assigning an initial velocity. A Modified Mohr-Coulomb model is used to capture the dilative response of sand based on its relative density. A parametric study is carried out for a range of relative density, critical state friction angle of the sand and impact velocity of the FFP. It was observed that the peak deceleration increases with increasing relative density, critical state friction angle, impact velocity and the mass of the penetrometer. The observed trend has been presented in simple charts and can be useful in interpretation of frictional property and state of near-surface sandy deposits.

Keywords: Coupled Eulerian Lagrangian, Modified Mohr-Coulomb, ball penetrometer, free fall penetration.

1 INTRODUCTION

FFPs are portable probes with housing for accelerometer, gyroscope and other instrumentation and are dropped on to the soil. The impact causes penetration in the soil which resists the probe's motion through mobilized shear strength, bringing it to halt. The recorded deceleration is used to calculate the dynamic resistance and obtain the soil parameters of interest. This simple test allows for the rapid characterization of a large area within a short time, giving an edge over the conventional push-in tests.

Methods to interpret the FFP deceleration data have been developed and advanced by conducting laboratory and field tests (e.g. Dayal and Allen, 1975, Stegmann et al., 2006, Stoll et al., 2007, Stark et al., 2009, Chow and Airey, 2013, Blake et al., 2016, White et al., 2018, Chow et al., 2023) with majority of them conducted in cohesive soils. FFP performance in sand is not extensively studied due to constraints like small penetration depth and complexity in data interpretation due to varying drainage conditions. Available literature (Akal and Stoll, 1995, Stark, et al., 2009, Albatal et al., 2020) have only considered the effect of some governing parameters on the peak deceleration (a_{peak}) after impact. Most of these studies were conducted using conical/torpedo shaped penetrometers. Spherical/Ball penetrometer has been used by researchers (Morton et al., 2016, Kadabinakatti et al., 2024) as it is unaffected by errors caused due to off-axis penetration (due to initial tilt at impact caused by underwater currents) of commonly used conical/torpedo shaped penetrometers.

There exists a clear lack of systematic study to assess the key parameters affecting peak deceleration of FFPs in sandy deposits. This study carries out parametric study on the effect of relative density, D_r, critical state friction angle, ϕ_{cv} of the sand and impact velocity, V of spherical FFPs on its peak deceleration. Coupled Eulerian Lagrangian (CEL) technique was used to avoid mesh distortion and convergence issues observed inherently in large deformation problems, in conjunction with a Modified Mohr-Coulomb (MMC) constitutive model to capture the strain dependent dilative response of the sand. A series of dynamic explicit analysis were run in Abaqus v6.14; Dassault Systèmes (ABAQUS 2014) to evaluate the effect of stated parameters on the penetration response.

.

2 NUMERICAL ANALYSIS

2.1 Geometry, mesh and boundary conditions

A 3-Dimensional soil domain (2m x 2m x 2.2m including void space) was modeled as a Eulerian mesh using the 8-node EC3D8R brick elements. The 3-Dimensional model was required because of the lack of axi-symmetric elements in CEL framework. The eulerian mesh allows the flow of material (sand) through it without deforming. The stainless steel spherical FFP was modelled as a lagrangian body meshed with C3D10M second order modified tetrahedral elements. To reduce the computational time and effort, only a quarter of the problem domain has been modelled using the symmetry about vertical z-axis passing through the centroid of FFP as shown in Figure 1. An additional void space was also modeled to capture the material flowing out of the top surface of the soil. Post mesh convergence, a minimum mesh size of 0.01 m was selected to avoid mesh dependency on the penetration response.

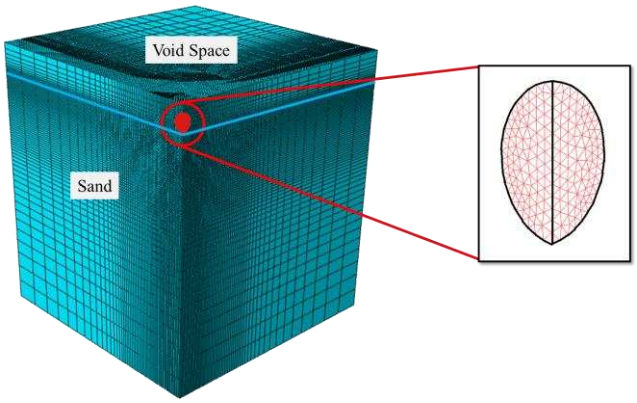

Figure 1. Abaqus model with discretized domain

2.2 Constitutive model

Modified Mohr-Coulomb (MMC) constitutive model adopted from Hu et al., 2015 is incorporated in the study through the VUSDFLD subroutine. It accounts for the dilative response with the cumulative plastic strain, capturing the hardening/softening behavior observed in sand. The incremental plastic strain $\varepsilon_{plastic}$ for any time increment is obtained by:

$$\varepsilon_{plastic} = \sqrt{\frac{2}{3}\{(\Delta\varepsilon_1 - \Delta\varepsilon_2)^2 + (\Delta\varepsilon_2 - \Delta\varepsilon_3)^2 + (\Delta\varepsilon_3 - \Delta\varepsilon_1)^2\}} \quad (1)$$

where $\Delta\varepsilon_1$, $\Delta\varepsilon_2$ and $\Delta\varepsilon_3$ are the change in principal plastic strains between two successive time increments.

The effect of dilation is accounted for by modifying the mobilzed friction angle as per Bolton (1986). Bolton, 1986 related the peak dilation and friction angle (ψ_p and ϕ_p) with relative density index, I_r ($0 < I_r \leq 4$) given by:

$$\phi_p = \phi_{cv} + A_\psi I_R \quad (2)$$

and,

$$\psi_p = 2A_\psi I_R \quad (3)$$

where ϕ_{cv} is the critical state friction angle, $A_\psi = 3$ (assuming the triaxial condition to hold valid) and

$$I_R = D_r\left(Q - ln\left\{\frac{100\,p'}{p_a'}\right\}\right) - R \quad (4)$$

with Q being a measure of crushing strength of the sand particle and R is a constant. For clean sands, $Q = 10$ and $R = 1$ is adopted. As reported in Hu et al., 2015, peak dilation is observed at ε_p (= 4%) and again becomes zero beyond threshold plastic strain, ε_{cv} (= 10%) for superfine silica sands. This was based on the triaxial tests conducted by Pucker et al. (2013). At this strain, the mobilized friction angle becomes equal to the critical state friction angle. Using the above set of equations, the peak dilation and peak friction angles are calculated. For the sake of simplicity, the initial friction angle was taken equal to the critical state friction angle.

2.3 Parametric Study

The deceleration response of a free-fall penetrometer is affected by FFP test parameters and soil properties. Series of simulations were run to assess the influence of key soil and FFP parameters on the peak deceleration, a_{peak}, deceleration profile and resistance profile throughout the depth of penetration. A range of impact velocity (V) of the penetrometer was chosen for different combinations of critical state friction angle (ϕ_{cv}) and relative density (D_r) of the sand. Table 1 summarizes the properties and values of different parameters adopted from Kezdi, 1974, Bowles and Guo, 1996, Teh et al., 2010 in the study.

Table 1. Key parameters used in the numerical model

Parameter	Value
Spherical FFP Parameters	
Sphere-Soil Interface Conditions	Frictionless
Sphere Diameter	0.1345 m
Mass of the sphere	10 kg
Density (ρ_{ss})	7850 kg/m^3
Impact Velocity	5,10, 15 & 20 m/s
Soil Parameters	
Poisson's ratio	0.33
Relative Density	20%, 35%, 50%, 65%, & 80%
Elastic Modulus	20, 30, 40, 52.5 & 65 MPa
e_{min}	0.449
e_{max}	0.747
ϕ_{cv}	25°, 30° & 35°

3 RESULTS AND DISCUSSIONS

3.1 Deceleration vs. time profile

The acceleration at the reference point for the rigid spherical FFP was obtained as output and plotted vs. time. Figure 2 shows typical acceleration-time profiles for two impact velocities at two different relative densities.

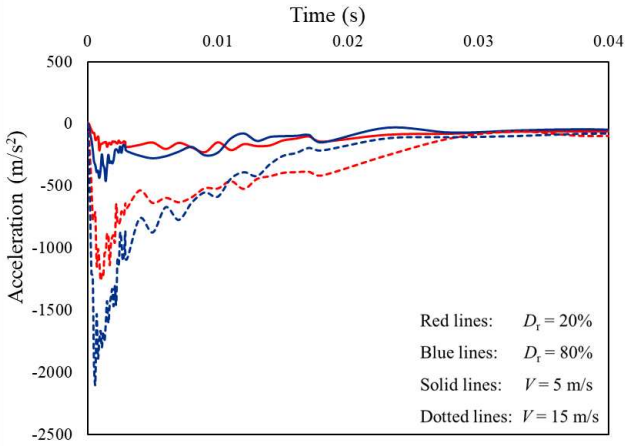

Figure 2 Deceleration vs. time plots (ϕ_{cv} = 35°)

It is observed that the deceleration reaches its peak value, a_{peak}, just after impact and then reduces to zero.

3.2 Effect of relative density and impact velocity

It is observed that peak deceleration increases with increasing impact velocity and relative density. Increasing relative density pronounces the dilatancy and hence, the mobilized peak friction as seen from Eqautions (2), (3) and (4). Dense sand therfore offers higher resistance and thus, higher peak deceleration values are noted as shown in Figure 3.

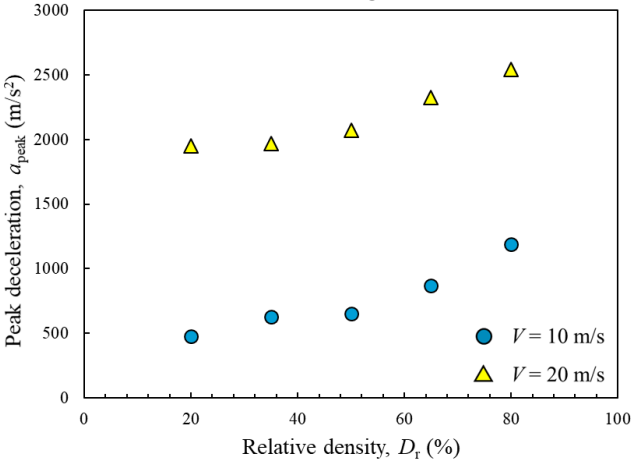

Figure 3 Relative density, D_r vs. peak deceleration, a_{peak} (ϕ_{cv} = 30°)

3.3 Effect of critical state friction angle

The critical state friction angle value directly influences the mobilized peak friction value, as inferred from Equation (2). Thus, a sand with higher ϕ_{cv} will offer a higher resistance/peak deceleration, as depicted in Figure 4.

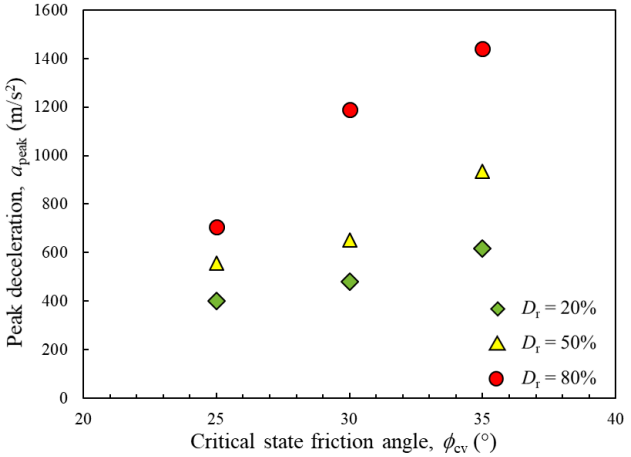

Figure 4 Critical state friction angle, ϕ_{cv} vs. peak deceleration, a_{peak} (V = 10 m/s)

3.4 Effect on duration of penetration

The exact duration of penetration could not be identified due to computational constraints and bouncing of FFP in the terminal stage of penetration. We define stoppage time t_{stop} as the first instance where

velocity of the FFP changes its direction. Figure 5 shows the variation in t_{stop} values with relative density and critical state friction angle for two impact velocities.

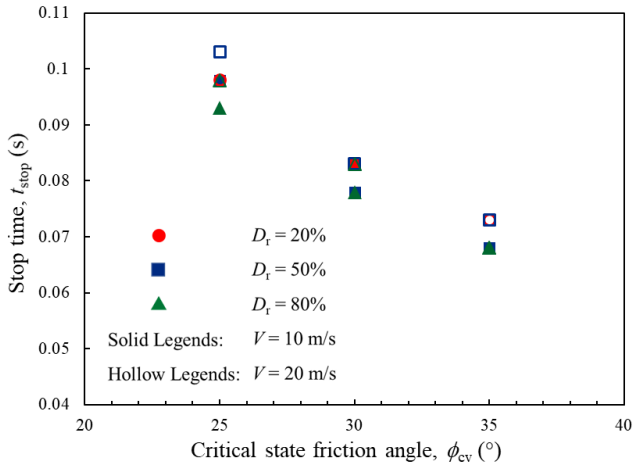

Figure 5 Variation in stoppage time, t_{stop} values

As observed from the above figure, the t_{stop} value reduces with increase in ϕ_{cv}, bringing the FFP to halt earlier. It is also interesting to note that the effect of relative density and impact velocity is minimal on the duration of penetration. The independence of t_{stop} on impact velocity has been reported by Ciamarra et al., 2004 for disks which was also validated by Goldman and Umbanhowar, 2008 for disks and spheres with impact velocities ≥ 1.5 m/s.

3.5 Soil resistance profiles

Dynamic soil resistance, R_{soil} was obtained from Newton's 2nd law of motion which, for an FFP penetrating in soil can be written as:

$$m\frac{dv}{dt} = W' - R_{soil} \qquad (5)$$

where m is the mass of FFP, v is the instantaneous velocity, dt is time increment and W' is the buoyant weight of the FFP. The resistance profile with depth follows a typical pattern for any combination of parameters as shown in Figure 6.

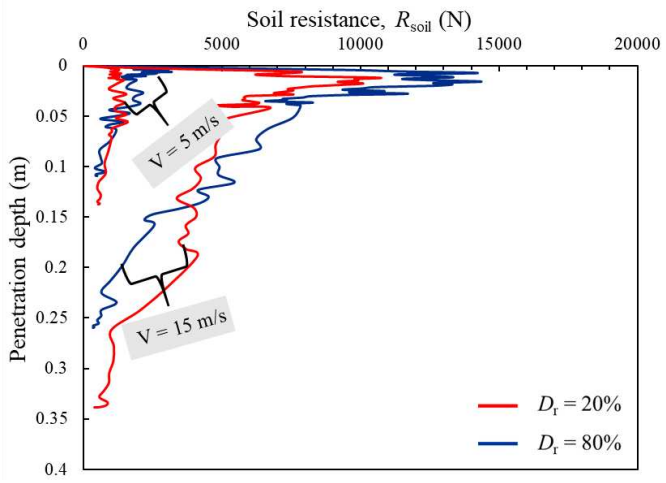

Figure 6 Dynamic resistance with depth (ϕ_{cv} = 30°)

3.6 Energy Dissipation profiles

The initial total energy, E_{ini} possessed by the FFP at the moment of impact is obtained by:

$$E_{ini} = 0.5mV^2 + mgd_p \qquad (6)$$

where g is the gravitational acceleration and d_p is the final penetration depth of the FFP. As the FFP advances through the soil, this energy dissipates mostly through itnergranular shearing and opening of a cavity in the soil. The energy dissipated/spent, E_{spent} till an instantaneous penetration depth z is obtained by the area under the resistance vs. depth curve (Figure 6), i.e.:

$$E_{spent} = \sum_{z=0}^{z=d_p} R_{soil}.\Delta z \qquad (7)$$

where Δz is the incremental depth between two successive time increments. E_{spent} at depth d_p calculated using Equation (7) may slightly differ (since this is a numerical approximation of the area under the curve) from E_{ini}. This difference was uniformly distributed throughout the depth to make initial and dissipated energy equal. Finally, plots of dissipated energy ratio, R (= E_{spent}/E_{ini}) with normalized penetration depth (z/d_p) were obtained as shown in Figure 7.

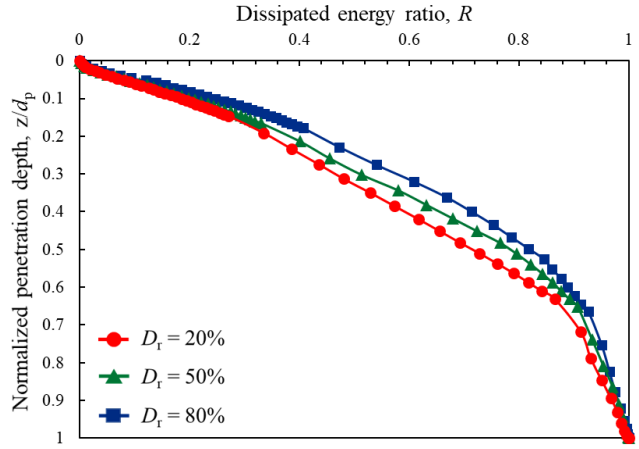

Figure 7 Dissipated energy profile with depth (V = 10 m/s & ϕ_{cv} = 35°)

It is clear from the above figure that for a given normalized penetration depth, more energy is dissipated by a dense sand (with higher relative density). The energy dissipation in the beginning (< 10% of d_p) however, seems to be marginally affected of the relative density of sand. Also visible from the curve is the sudden change in the slope of these curves at around 70% normalized penetration depth.

The slope of these curves is also dependent on the initial impact velocity, since this is a dynamic problem. Figure 8 shows the variation in energy dissipation profile with impact velocity for a typical relative density and critical state friction angle.

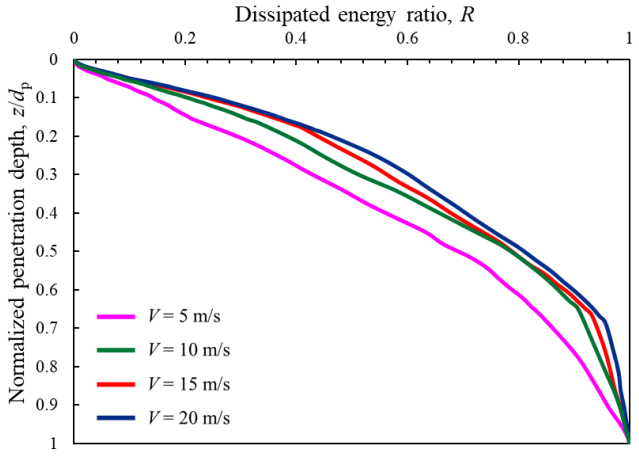

Figure 8 Variation of energy dissipation profiles with impact velocity (ϕ_{cv} = 35° & D_r = 50%)

The above figure again illustrates that for a given sand, FFP with higher impact velocity will lose energy at a faster rate.

4 CONCLUSION

This study explores the effect of relative density and critical state friction angle of sand and impact velocity of FFP on the penetration response.

It was observed that the peak deceleration increases with increase in D_r, ϕ_{cv} and V. The duration of penetration was observed to be independent of impact velocity and relative density but reduced with increasing critical state friction angle. The rate of energy dissipation with depth was found to be dependant on the relative density and could prove to be useful in estimating the packing of sand, although it was observed to vary with the impact velocity. Other interesting insights regarding the rate of energy loss also includes its independence on relative density in the initial penetration regime (< 10% of d_p) and sudden decrease near the end (≈ 70% of d_p).

These results are derived using a simple constitutive model and CEL technique assuming the sand to be dry and thus, have certain limitations. CEL, though useful for simulating large deformation problems, tends to be computationally expensive due to lack of axi-symmetric elements. The post-peak softening response might be affected by mesh size due to strain-localization, which has not been considered here. The effect of relative density and stress levels on the Poisson′s ratio was ignored in the current study. Also, the operative interface friction coefficient needs to be determined for this dynamic penetration problem, which might slightly alter the penetration response. Modeling the actual FFP in saturated sands will require supplementary techniques to capture pore pressure effects with appropriate drainage behavior.

Despite the stated limitations, these observations can lead to a better understanding of the mechanics of free-fall penetration problem and relate the penetration response with the shallow-depth properties of sand. With the use of a heavier FFP, the desired penetration depth can be achieved for offshore geotechnical engineering applications such as sediment transport, mine-burial, pipelines and risers, scour depth near offshore foundations etc.

AUTHOR CONTRIBUTION STATEMENT

A. Singh: Formal Analysis, Writing- Original draft. **S. Chatterjee**.: Methodology, Visualization, Supervision, Writing- Reviewing and Editing.

REFERENCES

ABAQUS. (2014). “Analysis user’s manual, version 6.14.” Providence, RI: *Dassault Systemes*, Simulia.

Albatal, A., Stark, N. and Castellanos, B. (2020). “Estimating in situ relative density and friction angle of nearshore sand from portable free-fall

penetrometer tests." *Canadian Geotechnical Journal* 57: 17-31.

Akal, T. and Stoll, R. D. (1995). "An expendable penetrometer for rapid assessment of seafloor parameters". *Proc. OCEANS'95: Challenges of our changing global environment*. Marine Technology Society/IEEE, Institute of Electrical and Electronics Engineers (IEEE), New York, 1822–1826.

Blake, A., O'Loughlin, C., Morton, J., O'Beirne, C., Gaudin, C. and White, D. (2016). "In situ measurement of the dynamic penetration of free-fall projectiles in soft soils using a low-cost inertial measurement unit." *Geotechnical Testing Journal*, 39(2), 235-251.

Bolton, M.D. (1986). "The strength and dilatancy of sands". *Géotechnique*, 36: 65–78.

Bowles, J. E., and Guo, Y. (1996). *Foundation analysis and design* (Vol. 5). New York: McGraw-hill.

Ciamarra, M. P., Lara, A. H., Lee, A. T., Goldman, D. I., Vishik, F. I., and Swinney, H. L. (2004). Dynamics of drag and force distributions for projectile impact in a granular medium. *Physical review letters*, 92(19), 194301.

Chow, S. H. and Airey, D. W. (2013). "Soil strength characterization using free falling penetrometers." *Géotechnique*, 63(13), 1131–1143.

Chow, S. H., O'Loughlin, C. D., Goh, C. L. V., McIlduff, R., White, D. J., and Chow, F. C. (2023). "A comparative field study of free-fall cone and sphere penetrometers in soft sediment." *Ocean Engineering*, 280, 114094

Dayal, U., and Allen, J. H. (1975). "The Effect of Penetration Rate on the Strength of Remolded Clay and Sand Samples." *Canadian Geotechnical Journal*, 12(3), 336-348.

Goldman, D. I., and Umbanhowar, P. (2008). Scaling and dynamics of sphere and disk impact into granular media. *Physical Review E—Statistical, Nonlinear, and Soft Matter Physics*, 77(2), 021308.

Hu, P., Wang, D., Stanier, S. A. and Cassidy, M. J. (2015). "Assessing the punch-through hazard of a spudcan on sand overlying clay." *Géotechnique*, 65(11), 883-896.

Kadabinakatti, S., Chatterjee, S., Basu, P., and Gamidi, S. H. (2024). Undrained shear strength estimation through instrumented free-fall penetration tests using spherical and conical penetrometers. *Ocean Engineering*, 309, 118489.

Kezdi A. and Rethati, L. (1974). *Handbook of soil mechanics* (Vol. 1). Amsterdam: Elsevier.

Morton, J. P., O'Loughlin, C. D. and White, D. J. (2016). "Estimation of soil strength in fine-grained soils by instrumented free-fall sphere tests." *Géotechnique*, 66(12), 959-968.

Pucker, T., Bienen, B. and Henke, S. (2013). "CPT based prediction of foundation penetration in siliceous sand." *Applied Ocean Research*, 41, 9-18.

Stark, N., Kopf, A., Hanff, H., Stegmann, S., and Wilkens, R. (2009). "Geotechnical investigations of sandy seafloors using dynamic penetrometers". Pages 1–10 in *Oceans'09*. Biloxi, MS.

Stegmann, S., Villinger, H. and Kopf, A. (2006). Design of a modular, marine free-fall cone penetrometer. *Sea Technology*, 47(2), 27–33.

Stoll, D., Sun, Y. F. and Bitte, I. (2007). "Seafloor properties from penetrometer tests." *IEEE Journal of Oceanic Eng*ineering, 32(1), 57–63.

Teh, K. L., Leung, C. F., Chow, Y. K. and M. J. Cassidy (2010). "Centrifuge model study of spudcan penetration in sand overlying clay. " *Géotechnique*, 60(11), 825-842.